Introduction to Numeric Simulation of Magnetic Fluid Flows

Ataias Pereira Reis, Yuri Dumaresq Sobral, Francisco Ricardo da Cunha
Universidade de Brasília
Departamento de Matemática
Brasília, Brasil
ataiasreis@gmail.com

***Abstract*—This work aims at studying how magnetic fluids behave in a 2D lid-driven cavity. In order to achieve this goal, a computer program was developed to solve the Navier-Stokes equation using finite differences. In addition to that, different equations for the evolution were introduced. The governing equations in continuous form and also in discrete form are presented, as well as the vectors fields resulted from computations. Solving the Poisson equation is done by means of an implicit method with sparse matrices and Cholesky factorization. Once the hydrodynamic and magnetostatic parts are solved, vector fields and streamlines are plotted for analysis of the flow. A few distinct Reynolds numbers are tested, as well as some different magnetic parameters. We observe that the magnetic field strongly influences the flow on the cavity.**

***Index Terms*—Magnetic fluid, Driven Cavity, Finite differences, Magnetohydrodynamics**

I. Introduction

This project aims at studying magnetic fluids in a 2D lid-driven cavity. The ideal cavity used here is a square whose side is equal to unity. All the boundaries but the top have null velocities. The lid has a stationary velocity pattern that will be presented. Even though this may seem a simplistic method, papers have been presented not only in the last century but also in this century to study real problems. Garandet [4] uses a similar approach to study solute segregations. On the field of biomagnetic fluids, Tzirtzilakis [9] has also considered a cavity and analyzed the stationary solutions under different conditions of the Reynolds numbers and magnetic parameters. Differently from this last work, our project has not considered a method to find directly the steady-state flow, but has evolved in discrete time steps from rest until the steady state is reached. The advantage is that more data can be analyzed, so that it is possible to know when vortices start to appear and if there are any that disappear during the evolution to steady-state. Animations were made in order to better examine those results.

A colloidal magnetic fluid, or ferrofluid, consists typically of a suspension of monodomain ferromagnetic particles such as magnetite in a nonmagnetic carrier fluid. Particle-to-particle agglomeration is avoided by surfactants covering the particles, and Brownian motion prevents particle sedimentation in gravitational or magnetic fields. [8]. Magnetic fluids have usually around 10^{23} magnetic nano-particles per cubic meter and are opaque at visible light since most of them are oil-based.

The differential equations will be solved using finite differences [7], a method that approximates each derivative by discrete terms involving differences. The domain in which the problem is to be solved must be turned into a mesh. The smaller the cells of the mesh, the better the finite differences solution will be. All the finite differences used here are of second order, which means that the error decays quadratically as the number of points in the mesh increases. The mesh that is being used is a staggered grid. In such a grid, not every information is stored in the same point. For instance, on the cell ij, the pressure will be in position $i + \frac{1}{2}j + \frac{1}{2}$, while velocity in the x direction will be $u_{ij+\frac{1}{2}}$ and the y direction will be $v_{i+\frac{1}{2}j}$. This avoids spurious pressure modes as described in [5]. A cell of this grid is presented in Figure 1, while the mesh is presented in Figure 2. The simulation will have to use all the round points presented, and almost all the velocities marked, except the extreme left and bottom ones. After the solution is obtained, an interpolation can be made to obtain the values at any specified point. We have chosen to plot all the results in the middle point of each cell. The pressure is already in that position, but the velocities are not. Therefore, averages were computed to obtain those values in the middle point.

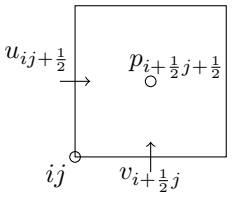

Fig. 1. Cell of the staggered grid

The code for the simulator was made with aid of programming language Julia, more information about this language is available at [3]. Julia offers several linear algebra packages that are easy to use and very efficient. Graphics were made using Python's graphical packages [6]. Codes and articles of this project are hosted on GitHub[1].

[1] https://github.com/ataias/ferrofluidos

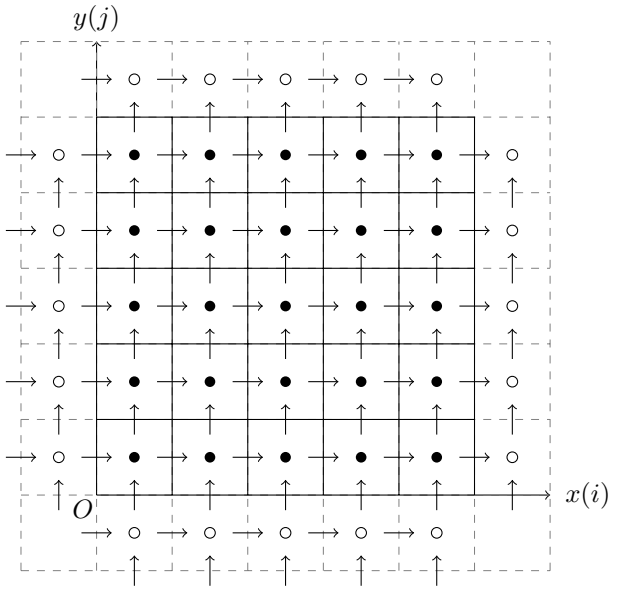

Fig. 2. Staggered-grid. Dark circles are internal points, while empty ones are part of the extra layer

II. Governing Equations

A. Hidrodynamics

Equations 1 and 2 govern the flow of an incompressible fluid. The first one is the Navier-Stokes equation [1], while the second one is the condition for incompressibility:

$$\left(\frac{\partial \mathbf{v}}{\partial t} + \mathbf{v}\cdot\nabla\mathbf{v}\right) = -\nabla p + \frac{1}{Re}\nabla^2\mathbf{v} + \mathbf{f}, \quad (1)$$

$$\nabla\cdot\mathbf{v} = 0. \quad (2)$$

In the latter equations, some terms are presented: $\mathbf{v}$ is the velocity, p stands for pressure and $\mathbf{f}$ is the force acting on the fluid, which is, in our case, created by a magnetic field. The Reynolds number Re is given by

$$Re = \frac{\rho L U}{\mu}, \quad (3)$$

in which ρ is the density of the fluid, L is a characteristic linear dimension, U is maximum speed in the cavity and μ is the dynamic viscosity.

Computer solutions require certain conditions on the time step and spacing of grid points. As well described on [5], the requirements are: stable diffusion,

$$\Delta t < \frac{1}{4} Re \Delta x^2, \quad (4)$$

stable advection, the CFL condition,

$$\Delta t < \frac{\Delta x}{U}, \quad (5)$$

and to resolve well the hydrodynamic boundary layer,

$$\Delta x < \frac{1}{Re}. \quad (6)$$

If the time-stepping conditions are not satisfied, the routine will try to solve the flow faster than the laws of physics allow. The result is an incorrect solution or divergency of the solution.

The Navier-Stokes equation is thorough, encompassing several types of flow. A specific solution is found by stating its boundary conditions. For the current work, the conditions are

$$u(x,1) = \sin^2(\pi x), \quad (7)$$

$$u(x,0) = u(0,y) = u(1,y) = 0, \quad (8)$$

$$v(x,0) = v(x,1) = v(0,y) = v(1,y) = 0. \quad (9)$$

B. Magnetism

Besides the hydrodynamics equations and conditions, the magnetic force in Equation 1, $\mathbf{f}$, must be computed. From Maxwell's theory, Equation 10 is obtained:

$$\nabla\cdot\mathbf{B} = 0. \quad (10)$$

and, from a magnetizable medium, we have Equation 11:

$$\mathbf{B} = \mu_0(\mathbf{M} + \mathbf{H}). \quad (11)$$

From the latter equations, it is possible to conclude that

$$\nabla\cdot\mathbf{H} = -\nabla\cdot\mathbf{M}. \quad (12)$$

The magnetostatic regime of the Maxwell's equations implies

$$\nabla\times\mathbf{H} = \mathbf{0}, \quad (13)$$

which indicates there is a potential field ϕ that satisfies

$$\mathbf{H} = -\nabla\phi. \quad (14)$$

With these last equations, it is possible to obtain

$$\nabla^2\phi = \nabla\cdot\mathbf{M}. \quad (15)$$

This is a Poisson equation that will give ϕ according the the local magnetization of the ferrofluid. The superparamagnetic case is being considered, what implies

$$\mathbf{M} = \chi\mathbf{H}. \quad (16)$$

Nevertheless, the potential ϕ cannot be introduced directly in the Navier-Stokes equation. What is needed is a relation that gives the magnetic force, which could then be incorporated in the fluid equations. The magnetic force is

$$\mathbf{f} = \mathrm{C_{pm}}\,\mathbf{M}\cdot\nabla\mathbf{H}, \quad (17)$$

in which $\mathrm{C_{pm}}$ is the magnetic Reynolds number, given by

$$\mathrm{C_{pm}} = \frac{\mu_0 H_0^2}{\rho u^2}. \quad (18)$$

The boundary conditions were not yet determined for the potential field ϕ. To derive those conditions, an applied magnetic field $\mathbf{H}$ was considered and the continuity

requirement was imposed for the normal component of **B**, Equation 11. This continuity can be mathematically represented by

$$(\mathbf{B}_{\text{out}} - \mathbf{B}_{\text{in}}) \cdot \mathbf{n} = 0. \tag{19}$$

From this, Equation 20 can be obtained:

$$\mu_0(H^{\text{n}}_{\text{out}} + M^{\text{n}}_{\text{out}}) \quad = \quad \mu_0(H^{\text{n}}_{\text{in}} + M^{\text{n}}_{\text{in}}). \tag{20}$$

The medium outside is air and therefore its magnetization $M^{\text{n}}_{\text{out}}$ is zero. The term $H^{\text{n}}_{\text{out}}$ is substituted following Equation 14, resulting in Equation 21:

$$\nabla\phi^{\text{n}}_{\text{d}} \quad = \quad -H^{\text{n}}_{\text{f}} + M^{\text{n}}_{\text{d}}. \tag{21}$$

From that, Neumann boundary conditions can be obtained for Equation 15. For the sake of clarity, they are presented in Equations 22 to 25. The subscripts are indicating matrix indices.

$$\left.\frac{\partial\phi}{\partial x}\right|_{\text{left}} \quad \approx \quad -H^x_{2,j} + M^x_{2,j} \tag{22}$$

$$\left.\frac{\partial\phi}{\partial x}\right|_{\text{right}} \quad \approx \quad -H^x_{n,j} + M^x_{n,j} \tag{23}$$

$$\left.\frac{\partial\phi}{\partial y}\right|_{\text{lower}} \quad \approx \quad -H^y_{i,2} + M^y_{i,2} \tag{24}$$

$$\left.\frac{\partial\phi}{\partial y}\right|_{\text{upper}} \quad \approx \quad -H^y_{i,n} + M^y_{i,n} \tag{25}$$

III. Solution Method

A. Time-splitting

In order to discretize the Navier-Stokes equation, an expansion is performed in directions x and y to obtain scalar equations and then finite differences of second order are applied. Nevertheless, a naive application of the discretized formulas will not yield a proper solution, as the fluid flow equation is highly non-linear due to its convective term $\mathbf{v} \cdot \nabla\mathbf{v}$. Also, pressure is not known in advance so, while it is needed at each time step, it is also an unknown that must be found. A method developed by Chorin, named time-splitting, and described in [2] was used to resolve this problem. Firstly, one starts by applying finite differences for the velocity derivative with respect to time and then manipulating by summing and subtracting $\mathbf{v}^*$ in the numerator, as in

$$\frac{\partial\mathbf{v}}{\partial t} \approx \frac{\mathbf{v}^{n+1} - \mathbf{v}^n}{\Delta t} = \frac{\mathbf{v}^{n+1} - \mathbf{v}^*}{\Delta t} + \frac{\mathbf{v}^* - \mathbf{v}^n}{\Delta t}, \tag{26}$$

in which $\mathbf{v}^n$ is the velocity at the current time-step and $\mathbf{v}^{n+1}$ is the velocity one time-step in the future.

The aforementioned technique imposes on the term $\frac{\mathbf{v}^{n+1}-\mathbf{v}^*}{\Delta t}$ of Equation 26 a relation with the pressure field:

$$\frac{\mathbf{v}^{n+1} - \mathbf{v}^*}{\Delta t} = -\nabla p. \tag{27}$$

Notice that Equation 27 already shows a relation between $\mathbf{v}^{n+1}$ and $\mathbf{v}^*$, a correlation that is pertinent because it is used to obtain the velocity in the next time step after pressure is calculated.

The other term, $\frac{\mathbf{v}^*-\mathbf{v}^n}{\Delta t}$, is responsible for all the terms of Equation 1, except the pressure gradient term that is already considered on Equation 27:

$$\frac{\mathbf{v}^* - \mathbf{v}^n}{\Delta t} \quad = \quad \frac{1}{Re}\nabla^2\mathbf{v} + \mathbf{f} - \mathbf{v} \cdot \nabla\mathbf{v} \tag{28}$$

The term $\mathbf{v}^*$ can be isolated in Equation 28 and then calculated easily as only known terms from time step n are involved in the aforementioned equation. Nevertheless, only time was discretized so far. Before any computation, we need to apply finite differences to Equation 28, which results in

$$\begin{aligned} u^*_{ij} \quad &= \quad u^n_{ij} + \Delta t\left[\frac{1}{Re}\left(\frac{u^s_{ij} - 4u^n_{ij}}{\Delta x^2}\right) + Fx^n_{ij}\right] + \\ &- \quad \left[u^n_{ij}(u^n_{i+1j} - u^n_{i-1j}) + \right. \\ &+ \quad \left. v^t_{ij}(u^n_{ij+1} - u^n_{ij-1})\right]\frac{\Delta t}{2\Delta x} \text{ and} \end{aligned} \tag{29}$$

$$\begin{aligned} v^*_{ij} \quad &= \quad v_{ij} + \Delta t\left[\frac{1}{Re}\left(\frac{v^s_{ij} - 4v^n_{ij}}{\Delta x^2}\right) + Fy^n_{ij}\right] \\ &- \quad \left[u^t_{ij}(v^n_{i+1j} - v^n_{i-1j}) + \right. \\ &+ \quad \left. v^n_{ij}(v^n_{ij+1} - v^n_{ij-1})\right]\frac{\Delta t}{2\Delta x}. \end{aligned} \tag{30}$$

In the latter equations, u^*_{ij} is the velocity in the x-direction at row i and column j in the mesh, while v^*_{ij} is the velocity in the y-direction with similar indexing. It is important to notice that those equations have truncated the 1/2 that would appear when the value is stored in the middle of the cell, or at the middle of a wall. In order to the computations to be valid, the values involved must be related to the same physical point. The terms u^t_{ij} and v^t_{ij} are interpolated velocities that need to be defined in order for the computations to be correct in the staggered-grid and are defined as:

$$u^t_{ij} \quad = \quad \frac{1}{4}(u^n_{ij} + u^n_{i+1j} + u^n_{i+1j-1} + u^n_{ij-1}), \tag{31}$$

$$v^t_{ij} \quad = \quad \frac{1}{4}(v^n_{ij} + v^n_{i-1j} + v^n_{i-1j+1} + v^n_{ij+1}). \tag{32}$$

The terms u^s_{ij} and v^s_{ij} refer to a sum of cell points around the corresponding velocity located in ij:

$$u^s_{ij} \quad = \quad u^n_{i+1j} + u^n_{i-1j} + u^n_{ij+1} + u^n_{ij-1}, \tag{33}$$

$$v^s_{ij} \quad = \quad v^n_{i+1j} + v^n_{i-1j} + v^n_{ij+1} + v^n_{ij-1}. \tag{34}$$

As a means to calculate p, the divergence operator is applied to both sides of Equation 27:

$$-\nabla \cdot \nabla p \quad = \quad \nabla \cdot \left(\frac{\mathbf{v}^{n+1} - \mathbf{v}^*}{\Delta t}\right). \tag{35}$$

As $\mathbf{v}^{n+1}$ has to obbey the incompressibility condition, its divergence is zero, with the remaining equation being transformed into a Poisson equation:

$$\nabla^2 p = \frac{1}{\Delta t}\nabla \cdot \mathbf{v}^*. \quad (36)$$

In order to solve Equation 36, its boundary conditions need to be determined. For that, the Navier-Stokes equation is expanded:

$$\frac{\partial u}{\partial t} + u\frac{\partial u}{\partial x} + v\frac{\partial u}{\partial y} = -\frac{\partial p}{\partial x} + \frac{1}{Re}\left(\frac{\partial^2 u}{\partial^2 x} + \frac{\partial^2 u}{\partial^2 y}\right) + f_x, \quad (37)$$

$$\frac{\partial v}{\partial t} + u\frac{\partial v}{\partial x} + v\frac{\partial v}{\partial y} = -\frac{\partial p}{\partial y} + \frac{1}{Re}\left(\frac{\partial^2 v}{\partial^2 x} + \frac{\partial^2 v}{\partial^2 y}\right) + f_y. \quad (38)$$

Equations 37 and 38 are valid in the whole domain, but to obtain the boundary conditions for p, these equations are evaluated only in the walls of the cavity. The conditions are those from Equations 7 to 9 and their application results in:

$$\left.\frac{\partial p}{\partial x}\right|_{\text{wall}} = \left.\frac{1}{Re}\frac{\partial^2 u}{\partial x^2}\right|_{\text{wall}} + f_x, \quad (39)$$

$$\left.\frac{\partial p}{\partial y}\right|_{\text{wall}} = \left.\frac{1}{Re}\frac{\partial^2 v}{\partial y^2}\right|_{\text{wall}} + f_y. \quad (40)$$

Equation 39 gives conditions for the left and right boundaries, while Equation 40 is for top and bottom. As the four walls have flux conditions, Neumann conditions, there are infinitely many solutions that differ only by a constant. Therefore, a point in the mesh is specified arbitrarily so that the program converges to a specific solution. This is allowed in our problem, as pressure itself is not directly needed, but only its gradient.

At this stage, $\mathbf{v}^*$ and p are known, so that $\mathbf{v}^{n+1}$ can be calculated by

$$\mathbf{v}^{n+1} = \mathbf{v}^* - \Delta t \cdot \nabla p. \quad (41)$$

Equation 41 is then used to evolve the system from time $n\Delta t$ to $(n+1)\Delta t$.

B. Poisson equations

The second step, solving for the pressure, can have an explicit or implicit solution method. Both methods were used, and the implicit one is much faster, so it is presented here. The hardest part of this method is that one can not apply the discretized equations directly, but it is necessary to form a linear system from it. For the implicit method, matrix A and vector b are needed to solve system $Ax = b$. The pressure elements are in the unknown x. This system gets very large, but most of the elements in matrix A are 0, so A is a sparse matrix. Firstly, let's present the steps to obtain A and b:

Consider a 5×5 grid as in Figure 3. The equation to be solved is Equation 42, a generic poisson equation.

$$\nabla^2 p = \frac{\partial^2 p}{\partial x^2} + \frac{\partial^2 p}{\partial y^2} = g(x, y) \quad (42)$$

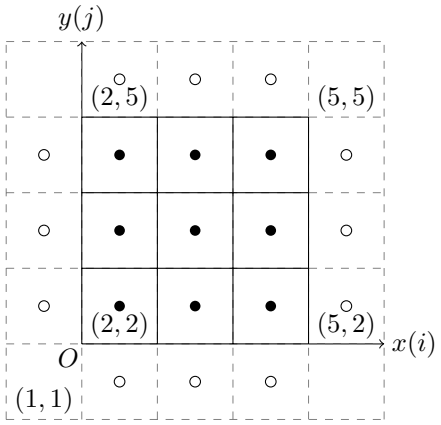

Fig. 3. Example grid to solve for pressure

Using second order central differences, Equation 43 is obtained. This equation is valid for internal points (black points in Figure 3).

$$\frac{p_{i-1j} - 2p_{ij} + p_{i+1j}}{\Delta x^2} + \frac{p_{ij-1} - 2p_{ij} + p_{ij+1}}{\Delta x^2} = g_{ij} \quad (43)$$

If term p_{ij} is isolated in Equation 43, an explicit equation is obtained to all the internal points. The external points will be obtained from boundary conditions. Nevertheless, what is needed is an implicit representation of the system. For that, all the equations need to be considered and then organized in matrix form. The first equations for the internal points are presented in Equations 44 to 46. Equations for the other internal points (more 6 equations) are easily obtainable.

$$-4p_{22} + p_{32} + \boldsymbol{p_{12}} + p_{23} + \boldsymbol{p_{21}} = \Delta x^2 g_{22} \quad (44)$$

$$-4p_{23} + p_{33} + \boldsymbol{p_{13}} + p_{24} + p_{22} = \Delta x^2 g_{23} \quad (45)$$

$$-4p_{24} + p_{34} + \boldsymbol{p_{14}} + \boldsymbol{p_{25}} + p_{23} = \Delta x^2 g_{24} \quad (46)$$

The pressure points written in bold letters are boundary points. This means there exists an equation that can account for them. There are twelve external points and from the boundary conditions it is easy to get the twelve equations. Equations 47 to 50 can have its indices substituted in order to get 12 equations.

$$\frac{\partial p}{\partial x}(0, y) = p_x(0, y) \approx (p_{2j} - p_{1j})/\Delta x \quad (47)$$

$$\frac{\partial p}{\partial x}(1, y) = p_x(1, y) \approx (u_{5j} - u_{4j})/\Delta x \quad (48)$$

$$\frac{\partial p}{\partial y}(x, 0) = p_y(x, 0) \approx (p_{i2} - p_{i1})/\Delta x \quad (49)$$

$$\frac{\partial p}{\partial y}(x, 0) = u_y(x, 0) \approx (p_{i5} - p_{i4})/\Delta x \quad (50)$$

From the 21 equations obtained, a rearrangement can be done to obtain matrix A, which is presented in Equation 51. The b vector is in Equation 52. Nevertheless, one of the Eigenvalues of this system is zero, so the matrix is not invertible. This problem has to do with the fact that

there are only Neumann boundary conditions and many differing-by-constant solutions are possible. To solve this problem, one value of the mesh must be imposed and the cell to be chosen can be any but one of the corner points, as they don't take any part on the equations.

$$\begin{bmatrix} -2 & 1 & 0 & 1 & 0 & 0 & 0 & 0 & 0 \\ 1 & -3 & 1 & 0 & 1 & 0 & 0 & 0 & 0 \\ 0 & 1 & -2 & 0 & 0 & 1 & 0 & 0 & 0 \\ 1 & 0 & 0 & -3 & 1 & 0 & 1 & 0 & 0 \\ 0 & 1 & 0 & 1 & -4 & 1 & 0 & 1 & 0 \\ 0 & 0 & 1 & 0 & 1 & -3 & 0 & 0 & 1 \\ 0 & 0 & 0 & 1 & 0 & 0 & -2 & 1 & 0 \\ 0 & 0 & 0 & 0 & 1 & 0 & 1 & -3 & 1 \\ 0 & 0 & 0 & 0 & 0 & 1 & 0 & 1 & -2 \end{bmatrix} \begin{bmatrix} p_{22} \\ p_{23} \\ p_{24} \\ p_{32} \\ p_{33} \\ p_{34} \\ p_{42} \\ p_{43} \\ u_{44} \end{bmatrix} = b \tag{51}$$

$$\begin{aligned} b &= \Delta x \begin{bmatrix} p_x\left(0, \frac{\Delta x}{2}\right) + p_y\left(\frac{\Delta x}{2}, 0\right) \\ u_x\left(0, \frac{3\Delta x}{2}\right) \\ p_x\left(0, \frac{5\Delta x}{2}\right) - p_y\left(\frac{\Delta x}{2}, 1\right) \\ p_y\left(\frac{3\Delta x}{2}, 0\right) \\ 0 \\ -p_y\left(\frac{3\Delta x}{2}, 1\right) \\ -p_x\left(1, \frac{\Delta x}{2}\right) + p_y\left(\frac{5\Delta x}{2}, 0\right) \\ -u_x\left(1, \frac{3\Delta x}{2}\right) \\ -p_x\left(1, \frac{5\Delta x}{2}\right) - p_y\left(\frac{5\Delta x}{2}, 1\right) \end{bmatrix} \\ &+ \Delta x^2 \left[g_{22}\ g_{23}\ g_{24}\ g_{32}\ g_{33}\ g_{34}\ g_{42}\ g_{43}\ g_{44}\right]^T \end{aligned} \tag{52}$$

For our problem, $p_{12} = 0$ was chosen. This updates one element of the matrix and one element of the vector. The updated values are shown in Equations 53 and 54.

$$A[1,1] = -3 \tag{53}$$

$$b[1] = p_y\left(\frac{\Delta x}{2}, 0\right)\Delta x + \Delta x^2 g_{22} \tag{54}$$

The equations just presented can be coded to define matrix A and vector b, but to actually obtain the vector x of pressure points the system must be solved. A sparse matrix solver available in Julia[2] is used. It uses a Cholesky factorization in order to solve the system. As the matrix is fixed, the factorization can be done once and for every other time-step the fatorized matrix is used. This is a performance-wise decision.

For the magnetism parts, it was only necessary to use finite differences on the governing equations. The Poisson implicit elements obtained in this section are also used for the magnetic part. The rest are explicit applications of the finite differences equations obtained.

IV. Results

It is important to validate the code. As part of the solution method, tests of the Poisson routine and of the discretization of the Navier-Stokes equation are made. The Poisson test is to check the error when comparing a computed result with the actual analytical function that solves the PDE. The second test applies to the Navier-Stokes equation and also for the Poisson one: verifying how the error decays according to an increase in mesh size. As all the discrete formulas used are of second order, this error should decay quadratically. The "Results" section will present both of these tests. Also, Navier-Stokes with magnetism will be tested to check the order of the discretization.

A. Validation of the Poisson Solver

The implementation of the solver was evaluated by testing a few different problems, but only a succinct presentation is done here with one problem: Equation 55.

$$\begin{cases} \nabla^2 u(x,y) = 0, \\ u_x(1,y) = \cos 2\pi y, \\ u_n(x,y) = 0, \text{otherwise, on the boundary.} \end{cases} \tag{55}$$

Its analytical solution is:

$$u(x,y) = \frac{\cosh 2\pi x}{2\pi \sinh 2\pi} \cos 2\pi y. \tag{56}$$

The Poisson validation routine returns the middle point difference on the grid that was found, this value is then divided by the real value on that point and multiplied by 100 to get a percentage. The maximum grid size used was 320×320. This one had an error smaller than 0.05%. The results for different grid sizes are presented in Figure 4. It is easy to see that the error decays quadratically, what was expected due to the second order finite differences that were used.

$$u(x,y) = \frac{\cosh 2\pi x}{2\pi \sinh 2\pi} \cos 2\pi y \tag{57}$$

B. Validation of the Navier-Stokes routine

Validation for the hydrodynamics is presented on Figure 5. Reynolds is chosen to be 40. The error will be compared against the solution of grid size 200×200, as access to the analytical solution is not possible. The important point to evaluate is that the error decays quadratically, what can be assessed from the image for simplicity. Vorticity was used instead of velocity because it is a scalar that accounts for both velocity terms. Note that the error corresponds to the base case of 200×200.

A similar test was used when magnetism is present. This case has a force $\mathbf{f}$ that differs from zero. Magnetic parameters chosen are $\chi = 0.5$, $C_{pm} = 0.8$, $\gamma = 3$ and a center for the magnetic field located close the left-bottom corner. The applied magnetic field is that of Figure 6. The error evolution for this case is presented on Figure 7. The values were compared in steady-state.

[2] http://julialang.org

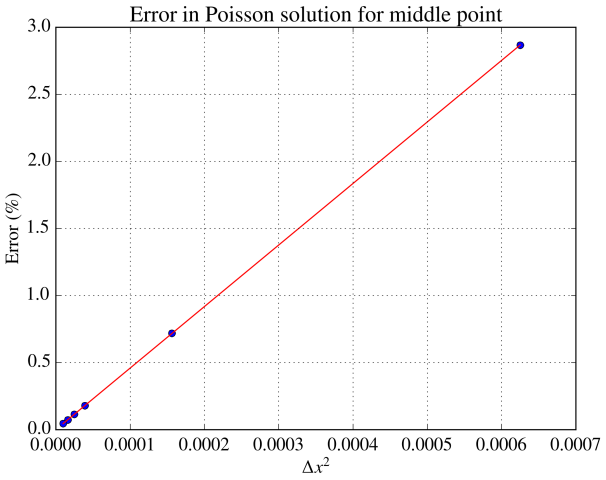

Fig. 4. Error evolving according to grid size. Higher grid sizes are closer to left-bottom corner. Error decays quadratically. Comparison with analytical solution. Grid sizes from 40×40 to 320×320.

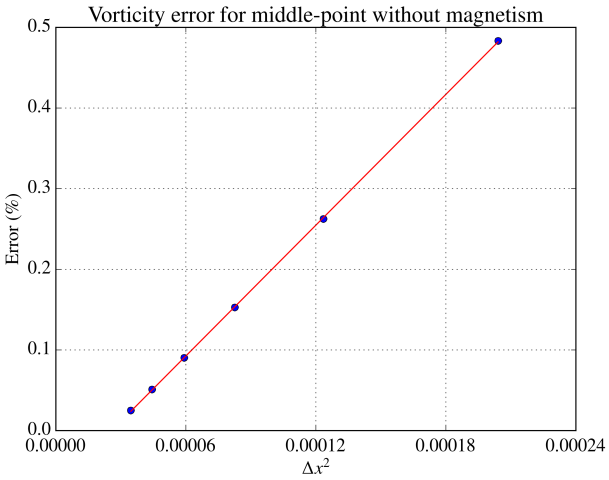

Fig. 5. Error evolving according to grid size. Higher grid sizes are closer to left-bottom corner. Error decays quadratically. Comparison with solution of 200×200 grid. Grid sizes from 70×70 to 170×170.

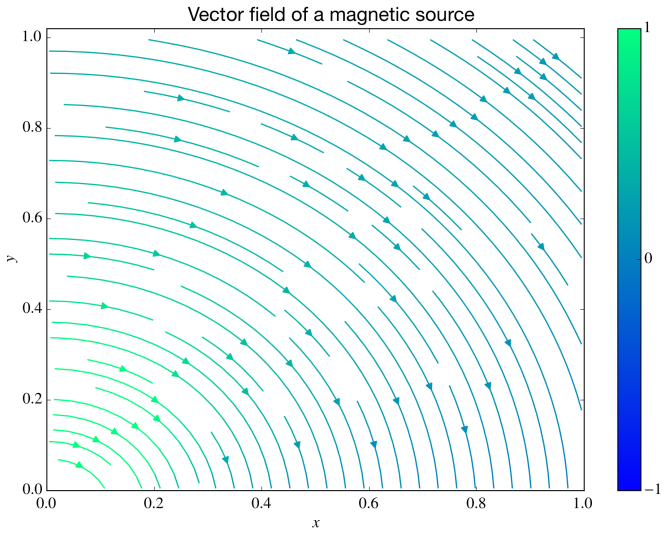

Fig. 6. Applied magnetic field. All tests were made with this specific magnetic field. γ values may change the actual intensity of field, but the streamlines are similar.

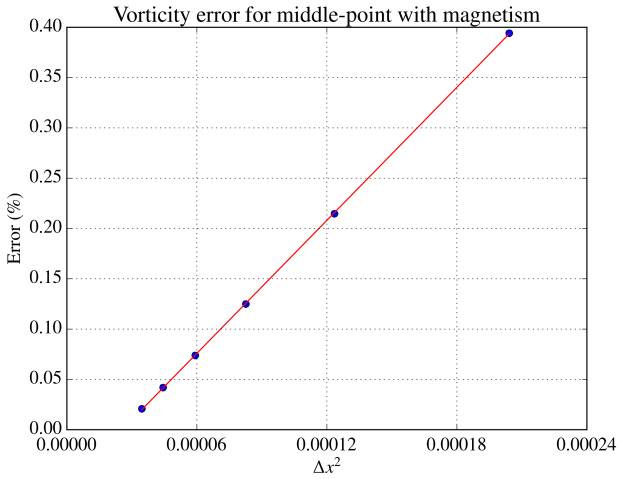

Fig. 7. Error evolving according to grid size. Higher grid sizes are closer to left-bottom corner. Error decays quadratically. Comparison with solution of 200×200 grid. Grid sizes from 70×70 to 170×170.

C. Preliminary studies of flow patterns

We have performed some tests to assess the influence of the dimensionless parameters Re and C_{pm} on the steady-state regimes that were obtained. Some Reynolds numbers were chosen and then several tests were executed for some fixed magnetic parameters. The magnetic parameters are $\chi = 0.5$, $C_{pm} = 0.8$ and $\gamma = 3.5$. Reynolds numbers presented here are 1, 50 and 100. Figures 8 to 19 present streamlines for the velocity and contour lines for the pressure. Images with magnetic parameters set to 0 are the ones without magnetization. All results are in steady state. We have also coded a routine to calculate the angle between $\mathbf{M}$ and $\mathbf{H}$ for every point in those simulations but, for the case presented here, this is not relevant, as $\mathbf{M} = \chi\mathbf{H}$ is one consideration for the magnetization in the current work (superparamagnetic regime).

Regarding the results with no magnetic field, Figures 8 to 18 present very similar results. Although the Reynolds number changes by a factor of 100, no major changes in the steady state flow were able to be observed. It is noticeable, though, that the flow is more asymmetric and the center of the main vortex shifts to the right as Re increases.

This changes dramatically when a magnetic field is in action. A small vortex already appears in Figure 9 and just grows larger as the Reynolds number increases up to 100 (Figures 11 and 13). Pressure also varies much more and a particular concentration of contour lines is observable close to the origin (the magnetic field is applied just a little off the origin) as presented in Figures 15, 17 and 19.

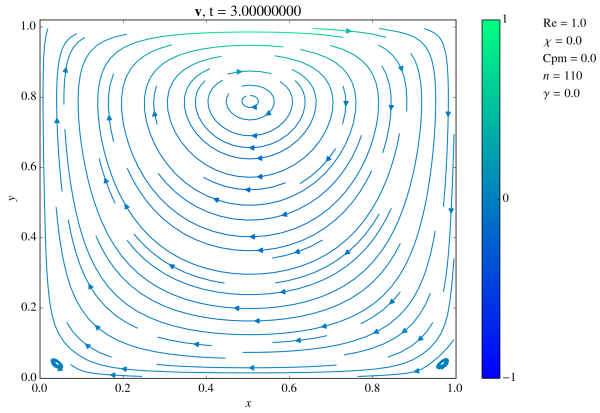

Fig. 8. Steady state solution without magnetic field, $Re = 1$. No extra vortices appear.

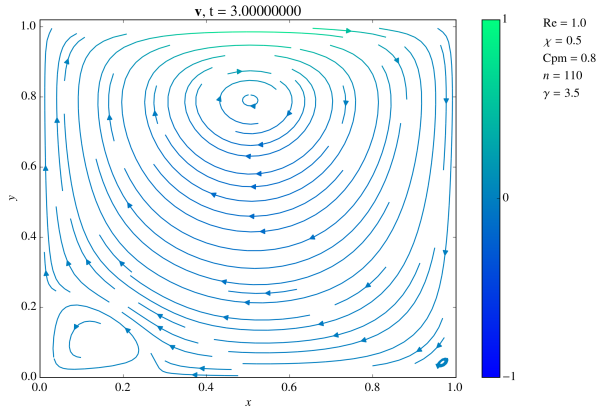

Fig. 9. Steady state solution without magnetic field, $Re = 1$. A new vortex starts to appear.

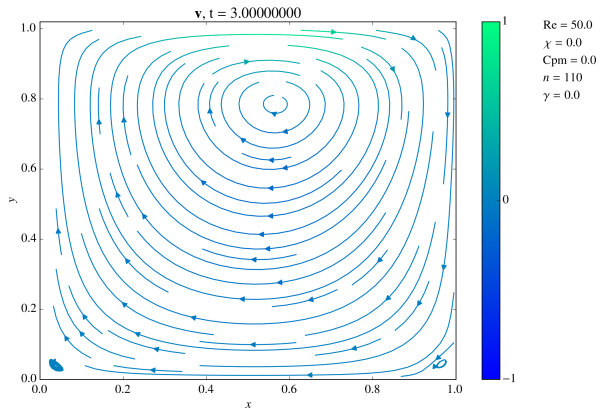

Fig. 10. Steady state solution without magnetic field, $Re = 50$. No extra vortices appear.

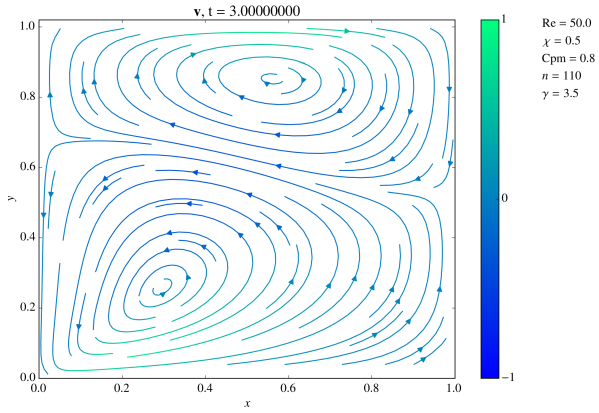

Fig. 11. Steady state solution without magnetic field, $Re = 50$. The new vortex is already bigger than the initial one.

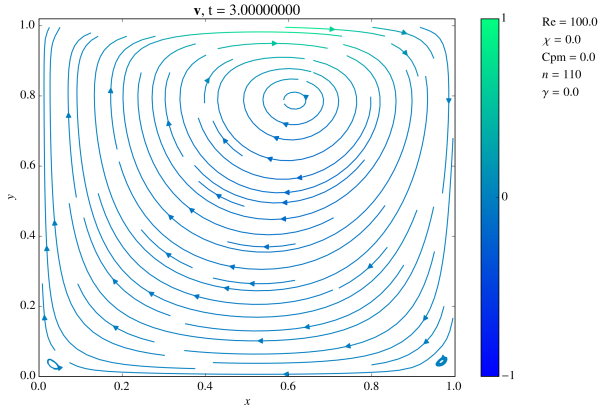

Fig. 12. Steady state solution without magnetic field, $Re = 100$. No extra vortices appear.

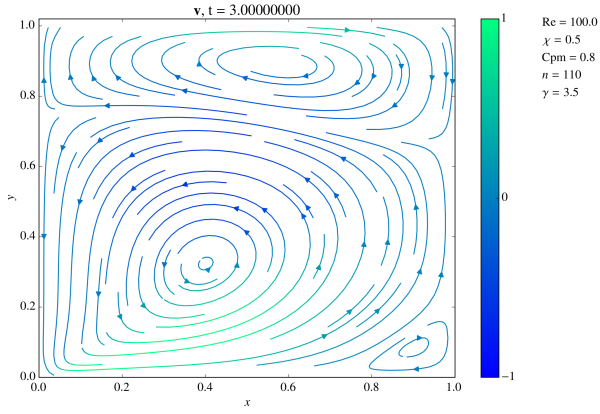

Fig. 13. Steady state solution without magnetic field, $Re = 100$. Vortex increased in comparison with $Re = 50$.

V. Conclusion

It is important for the code to be correct, otherwise it is meaningless to analyze the simulation results. The validation step shows that certainly the system is behaving as second order.

Although not presented in the last sections, it is interesting to observe that one problem that appeared was when physics was disregarded. Trying to apply an arbitrary magnetic field has a good chance of generating results that

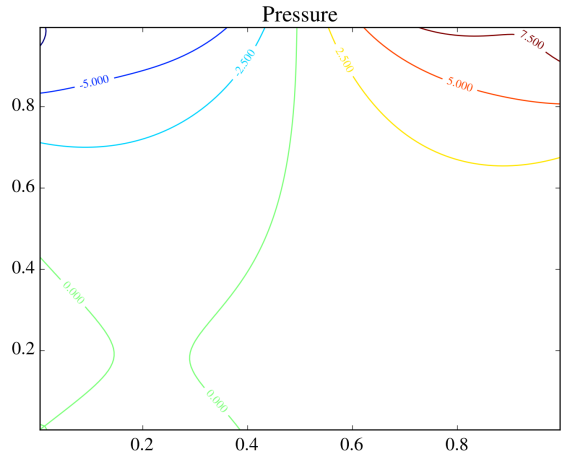

Fig. 14. Contour plot for pressure of the flow in Figure 8, $Re = 1$, no magnetism.

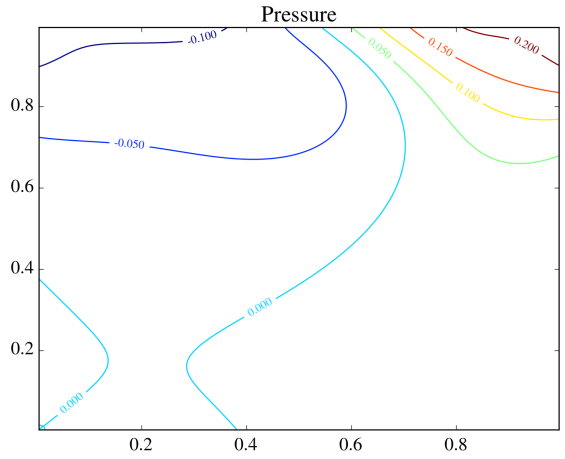

Fig. 16. Contour plot for pressure of the flow in Figure 10, $Re = 50$, no magnetism

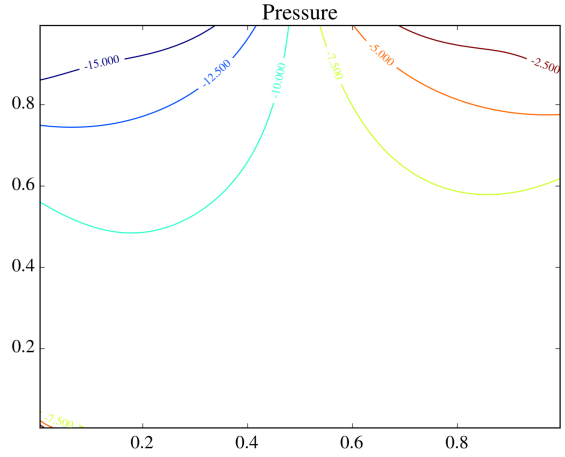

Fig. 15. Contour plot for pressure of the flow in Figure 9, $Re = 1$, with magnetism

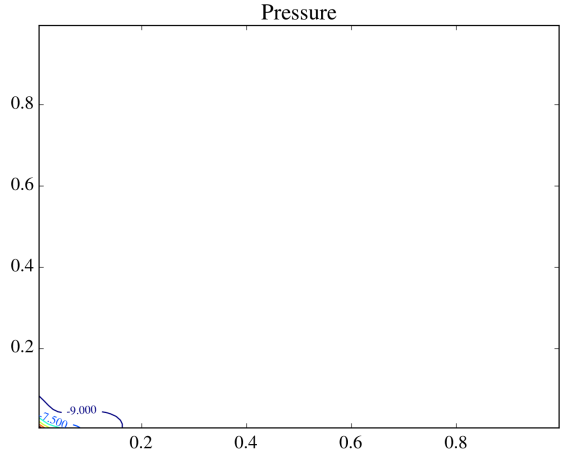

Fig. 17. Contour plot for pressure of the flow in Figure 11, $Re = 50$, with magnetism

converge but are incorrect when the governing equations are checked. The results presented comply to the laws that we claim to be following. This is also good evidence of correctness.

This work was a challenge in the aspect that an analytical solution was not available to check against, so it is important to state the importance of the validation step. The results were satisfactory and the tools here coded for exploring magnetic fluids are starting to get usable, when compared with the stage of one year ago.

VI. Future work

The results presented do not include Reynolds greater than 100 because the code is not currently abiding by any upwind scheme. This is something that is planned to be implemented. Also, a different magnetic field will be used, particularly the one of a Neodymium magnet, instead of the magnetic field of a wire, as used here.

Most importantly, we want to implement the dynamic evolution equations for the magnetization of the ferrofluid that are coupled with the flow field. This will certainly change significantly the dynamics of the flow and will be the subject of our next project.

Acknowledgments

Firstly, I thank God for this opportunity. I appreciate professor Yuri Dumaresq for his orientations so that this work could be done. Also, many thanks to CNPq for the scholarship.

References

[1] G.K. Batchelor. An Introduction to Fluid Dynamics, 1967.
[2] Alexandre Joel Chorin. A numerical method for solving incompressible viscous flow problems. *Journal of Computational Physics*, 135(2):118 – 125, 1997.
[3] NumFocus Foundation. The Julia Language. Available at http://julialang.org, version 0.3.11.

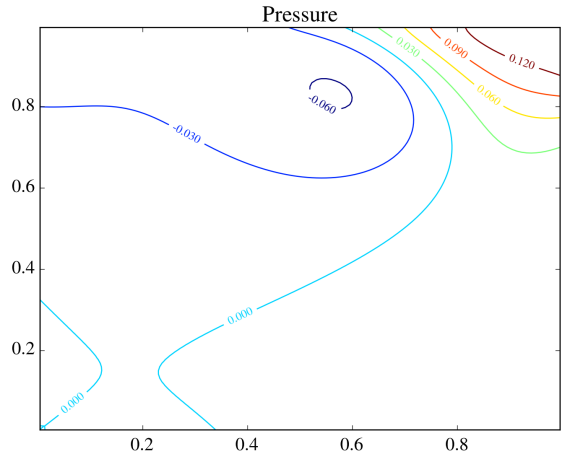

Fig. 18. Contour plot for pressure of the flow in Figure 12, $Re = 100$, no magnetism

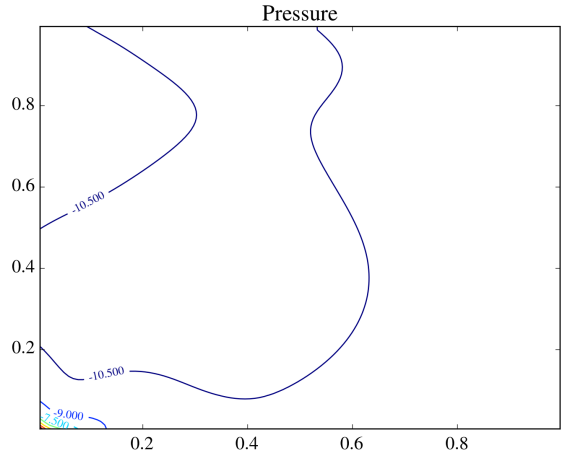

Fig. 19. Contour plot for pressure of the flow in Figure 13, $Re = 100$, with magnetism

[4] J.P. Garandet, N. Kaupp, D. Pelletier, and Y. Delannoy. Solute segregation in a lid driven cavity: Effect of the flow on the boundary layer thickness and solute segregation. *Journal of Crystal Growth*, 340(1):149 – 155, 2012.

[5] E.J. Hinch. Lecture notes on computational methods in fluid dynamics: Part i - a first problem., 2006.

[6] Eric Firing Michael Droettboom John Hunter, Darren Dale and the matplotlib development team. matplotlib: python plotting. Available at http://matplotlib.org, version 1.4.3.

[7] L.M. Milne-Thomson. The calculus of finite differences. London: Macmillan & Co., Ltd. XIX, 558 S., 23 Fig. (1933)., 1933.

[8] R E Rosensweig. Magnetic fluids. *Annual Review of Fluid Mechanics*, 19(1):437–461, 1987.

[9] E.E. Tzirtzilakis and M.A. Xenos. Biomagnetic fluid flow in a driven cavity. *Meccanica*, 48(1):187–200, 2013.